

¹¹C-GSK189254: A Selective Radioligand for In Vivo Central Nervous System Imaging of Histamine H₃ Receptors by PET

Christophe Plisson¹, Roger N. Gunn¹, Vincent J. Cunningham¹, Dirk Bender², Cristian A. Salinas¹, Andrew D. Medhurst³, Jennifer C. Roberts³, Marc Laruelle¹, and Antony D. Gee¹

¹GlaxoSmithKline, Clinical Imaging Centre, Hammersmith Hospital, London, United Kingdom; ²PET Center, Aarhus University Hospital, Aarhus C, Denmark; and ³GlaxoSmithKline, Neurosciences Centre of Excellence for Drug Discovery, New Frontiers Science Park, Harlow, United Kingdom

The histamine H₃ receptor is a G-protein-coupled presynaptic auto- and heteroreceptor whose activation leads to a decrease in the release of several neurotransmitters including histamine, acetylcholine, noradrenaline, and dopamine. H₃ receptor antagonists such as 6-[(3-cyclobutyl-2,3,4,5-tetrahydro-1*H*-3-benzazepin-7-yl)oxy]-*N*-methyl-3-pyridinecarboxamide hydrochloride (GSK189254) can increase the release of these neurotransmitters and thus may offer potential therapeutic benefits in diseases characterized by disturbances of neurotransmission. The aim of this study was to synthesize and evaluate ¹¹C-labeled GSK189254 (¹¹C-GSK189254) for imaging the histamine H₃ receptor in vivo by PET. **Methods:** GSK189254 exhibits high affinity (0.26 nM) and selectivity for the human histamine H₃ receptor. Autoradiography experiments were performed using ³H-GSK189254 to evaluate its in vitro binding in porcine brain tissues. GSK189254 was labeled by *N*-alkylation using ¹¹C-methyl iodide in good yields, radiochemical purity, and specific activity. A series of PET experiments was conducted to investigate ¹¹C-GSK189254 binding in the porcine brain. **Results:** In vitro autoradiography demonstrated specific ³H-GSK189254 binding in the porcine brain; therefore, ¹¹C-GSK189254 was evaluated in vivo in pigs and showed good brain penetration and high uptake in regions such as the striatum and cortices, known to contain high densities of the histamine H₃ receptors. The radioligand kinetics were reversible, and quantitative analysis was achieved with a 2-tissue-compartmental model yielding the distribution volume as the outcome measure of interest. The distribution volume was reduced to a homogeneous level in all regions after blocking by the coadministration of either unlabeled GSK189254 or ciproxifan, a structurally distinct histamine H₃ antagonist. Further coadministration studies allowed for the estimation of the radioligand affinity (0.1 nM) and the density of histamine H₃ receptor sites in the cerebellum (0.74 nM), cortex (2.05 nM), and striatum (2.65 nM). **Conclusion:** These findings suggest that ¹¹C-GSK189254 possesses appropriate characteristics for the in vivo imaging of the histamine H₃ receptor by PET.

Key Words: PET; ¹¹C; histamine H₃; GSK189254; pig

J Nucl Med 2009; 50:2064–2072

DOI: 10.2967/jnumed.109.062919

Histamine exerts a neurotransmitter function in both the central nervous system (CNS) and the periphery via the activation of 4 distinct histamine receptor subtypes: H₁, H₂, H₃, and H₄. The histamine H₃ receptors are widely expressed in the mammalian brain, with the highest densities found in areas involved in cognitive processes and arousal such as the cerebral cortex, hippocampus, basal ganglia, and hypothalamus (1,2). The histamine H₃ receptor has been reported to play a role in the regulation of the release and synthesis of histamine (3) and also the release of other neurotransmitters such as acetylcholine (4), noradrenaline (5), and dopamine (6).

CNS H₃ receptors have been implicated in the normal and pathophysiology of sleep and wakefulness (7), food intake (8), Alzheimer disease (9), schizophrenia (10), narcolepsy (11), epilepsy, cognitive disorders, and attention-deficit hyperactive disorder (7).

Most of this evidence comes from studies of laboratory animals or postmortem human brains. To further elucidate the CNS histamine H₃ receptor function in living humans, a noninvasive in vivo probe of the H₃ receptor is required. A large number of H₃ receptor ligands such as thioperamide (12), FUB372 (13), and ciproxifan (13,14) and radioligands such as ¹²⁵I-iodoproxifan (15) have been described in the literature as in vitro tools for binding studies. Potential PET and SPECT radioligands have also been reported (16–18); however, for diverse reasons, none of these radiotracers has been shown to be suitable as PET or SPECT ligands for brain imaging of the H₃ receptor. For example, ¹²³I-GR190028, ¹²³I-FUB271, ¹⁸F-FUB272, ¹¹C-UCL1829, and ¹⁸F-VUF5000 showed low brain uptake, and some of these compounds failed to show a heterogeneous distribution (¹²³I-FUB271, ¹⁸F-FUB272, ¹¹C-UCL1829) or saturable binding

Received Feb. 27, 2009; revision accepted Sep. 2, 2009.

For correspondence or reprints contact: Christophe Plisson, GlaxoSmithKline, Clinical Imaging Centre, Imperial College, Hammersmith Hospital, Du Cane Rd., London W12 0NN, U.K.

E-mail: Christophe.2.plisson@gsk.com

COPYRIGHT © 2009 by the Society of Nuclear Medicine, Inc.

(^{123}I -iodoproxifan, ^{18}F -VUF5000). Recently, an ^{11}C -labeled morpholine derivative (JNJ-10181457) and ^{18}F -labeled fluoro-proxifan were also evaluated in rats as potential PET ligands for this target. ^{11}C -JNJ-10181457 showed no clear evidence of H_3 receptor-specific binding in vivo in the rat brain (19). ^{18}F -fluoroproxifan showed a heterogeneous distribution; however, its binding could not be blocked in the cortical regions, suggesting either too high nonspecific binding or too low radioligand affinity for a measurable cortical signal (20). More recently, Hamill et al. described 2 new H_3 inverse-agonist PET radioligands that look promising for imaging and quantifying H_3 receptors (21).

6-[(3-cyclobutyl-2,3,4,5-tetrahydro-1*H*-3-benzazepin-7-yl)oxy]-*N*-methyl-3-pyridinecarboxamide hydrochloride (GSK189254) was recently described as a highly potent and selective H_3 receptor antagonist or inverse agonist (22). This good pharmacologic profile, combined with a chemical structure compatible with introducing an ^{11}C radiolabel, made this compound an interesting PET tracer candidate. The present work describes the labeling of GSK189254 with ^{11}C , the in vitro evaluation of its tritiated analog in the porcine brain, and the preliminary in vivo evaluation of ^{11}C -GSK189254 in the porcine brain as a PET agent candidate for the histamine H_3 receptor.

MATERIALS AND METHODS

Chemistry

Solvents were of high-performance liquid chromatography (HPLC) grade and were purchased from Aldrich or Merck. Labeling reactions were performed using anhydrous Sure/Seal solvent from Aldrich. The ^{11}C - CO_2 was produced using the GE Healthcare PETtrace 200 cyclotron. The preparation of ^{11}C -methyl iodide was achieved using a PETtrace MeI system (GE Healthcare). The labeling procedure was performed using a fully automated system (Synthia (23)) including the methylation step, HPLC purification, rotary evaporation, and labeled product formulation.

GSK189254 and its precursor for radiolabeling, 6-[(3-cyclobutyl-2,3,4,5-tetrahydro-1*H*-3-benzazepin-7-yl)oxy]-pyridinecarboxamide (**1**), were synthesized according to a published procedure (Fig. 1) (24).

Radiochemical Synthesis of ^{11}C -GSK189254 (25)

^{11}C -GSK189254 was prepared by *N*-alkylation of the carboxamide precursor **1** using cyclotron-produced ^{11}C -methyl iodide (Fig. 1). ^{11}C - CO_2 was produced by the $^{14}\text{N}(\text{p},\alpha)^{11}\text{C}$ nuclear reaction using a nitrogen gas target (containing 1% oxygen) pressurized to 150 psi and bombarded with 16.5-MeV protons. Subsequently, ^{11}C - CO_2 was converted into ^{11}C - CH_3I by catalytic reduction (Ni), which gave the ^{11}C - CH_4 intermediate, followed by gas phase iodination with iodine. The precursor **1** (1.0 mg) dissolved in dimethylsulfoxide (300 μL) was placed in a 1-mL glass vial. Tetrabutylammonium fluoride (20 μL) was added. The ^{11}C - CH_3I was passed in a stream of helium gas through the solution containing the precursor at room temperature. After the ^{11}C - CH_3I was delivered, the sealed vessel was heated at 130°C for 5 min and injected onto the semipreparative HPLC column (250 \times 10 mm) (Sphereclone ODS(2) C-18; Phenomenex). HPLC purification was performed at a 10 mL/min flow rate, with a mobile phase consisting of

acetonitrile and a solution of ammonium formate (50 mM) (42:58). The product fraction collected after approximately 7.7 min was evaporated to dryness and reformulated in 10 mL of 0.9% NaCl. Quality control was performed on a Sphereclone ODS(2) C-18 (250 \times 4.6 mm) or a Zorbax SB-C18 (150 \times 4.6 mm; Agilent) using acetonitrile and a solution of ammonium formate (50 mM) (48:52) as mobile phase at a flow rate of 3 mL/min or 1.0 mL/min, respectively. To confirm the radiopharmaceutical identity, the dose was also spiked with a GSK189254 standard.

Lipophilicity Measurements

Measurement of the partition coefficient of the radiolabeled compound was performed according to the method described by Wilson et al. using phosphate-buffered saline (phosphate buffer, 0.01 M; NaCl, 0.138 M; and KCl, 0.0027 M) at pH 7.4 and 1-octanol (26). The 1-octanol phase was washed with the buffer solution before any lipophilicity determination to reduce the potential errors due to hydrophilic impurities. Two measurements were performed from 2 different ^{11}C -GSK189254 productions, each consisting of 4 samples.

In Vitro H_3 Receptor Autoradiography

To assess the in vitro imaging properties of GSK189254, the preparation of ^3H -GSK189254 for autoradiography (specific activity, 3 GBq/ μmol [81 Ci/mmol]) was outsourced to Amersham Biosciences. Autoradiographic studies were based on a previously reported method (27). Frozen sagittal sections (20 μm) of porcine brain (Yorkshire/Danish Landrace; \sim 40 kg) were thaw-mounted onto gelatin-coated slides, and the slides were stored at -80°C until the time of assay. The sections were incubated in assay buffer (50 mM Tris-HCl, pH 7.7, and 5 mM ethylenediaminetetraacetic acid) containing 1 nM ^3H -GSK189254 for 60 min at room temperature (22°C). On anatomically adjacent sections, nonspecific binding was determined in the presence of 10 μM imetit. After incubation, all sections were rinsed 5 times for 3 min at 4°C in Tris-HCl buffer with the addition of 5 mM MgCl_2 . The sections were then quickly dipped in distilled water at 4°C to remove buffer salts, and they were dried in a stream of cool air. Once dried, the sections were apposed to Hyperfilm (Amersham) and exposed for 3 wk. After development, the film was analyzed using ANALYSIS imaging software (Olympus Soft Imaging Solutions). Adjacent sections were also stained with cresyl fast violet to allow for anatomic orientation.

Porcine PET Studies

All animal studies were performed in accordance with the Danish Animal Experimentation Act on a license granted by the Danish Ministry of Justice. Five Yorkshire/Danish Landrace pigs (\sim 40 kg) were housed singly in thermostatically controlled (20°C) and naturally illuminated stalls and were scanned under terminal anesthesia. The animals were medicated in advance with an intramuscular injection of 50 mg of midazolam and 250 mg of (*S*)-ketamine. The anesthesia was induced by an intravenous injection of 50 mg of midazolam and 125 mg of (*S*)-ketamine and maintained by ventilation with isoflurane (2%) in an $\text{O}_2/\text{N}_2\text{O}$ mixture (1/2). At the end of the scanning session, the pigs were euthanized by intravenous administration of an overdose of pentobarbitone.

After anesthesia was induced, the left femoral artery and vein of each animal were surgically cannulated (Avanti, size 4–7 French; Cordis Corporation). Blood samples were collected from the femoral artery, and the radiolabeled and nonlabeled agents were injected in the femoral vein. Animals were placed supine in

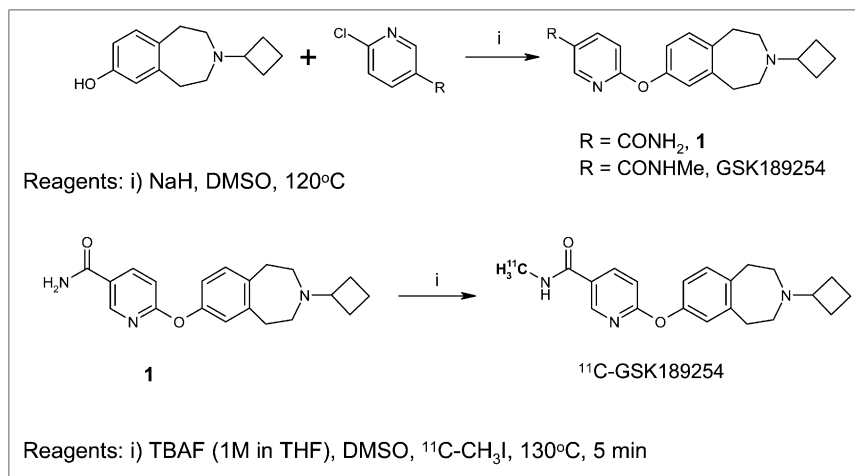


FIGURE 1. Radiosynthesis of ¹¹C-GSK189254.

a Siemens ECAT EXACT HR tomograph, with the head immobilized in a custom-made holding device. During the study, blood pH, *p*CO₂, and *p*O₂ levels were monitored and maintained within the normal physiologic range. In addition, blood pressure and heart rate were recorded throughout the study. In each PET experiment, 150–450 MBq of ¹¹C-GSK189254, which corresponded to an injected mass dose of GSK189254 of less than 2 μg, were administered intravenously in the femoral vein as a 1-min bolus injection. PET and arterial blood sampling commenced at the start of the radioligand administration. Dynamic emission data were collected in 3-dimensional mode for 90 min (26 frames; 8 × 0.25 min, 4 × 0.5 min, 2 × 1 min, 2 × 2 min, 4 × 5 min, and 6 × 10 min). For each study, the baseline PET summed image was coregistered with a 12-parameter affine registration to the Landrace porcine brain atlas using a mutual information metric. T1-weighted MRI scans from 22 female Yorkshire/Landrace pigs were used to generate an atlas according to methods described previously for the Gottingen minipig (28). Subsequently, the transformation parameters were applied to each frame in the dynamic image of all the PET scans acquired in that study. All registrations were assessed by visual inspection, and then the regional regions of interest (ROIs) were applied to the dynamic images to generate regional time-activity curves.

The present work was performed using 5 different pigs and consisted of a total of 14 scans. In each pig, a baseline scan was acquired before the administration of the challenge. The unlabeled drugs were all coadministered with the bolus injection of the radioligand. One animal received a 50-μg dose of GSK189254 per kilogram.

Two animals underwent scans involving the coadministration of ciproxifan: In the first animal, a PET measurement scan was acquired after the administration of each of 3 escalating doses of ciproxifan (0.006, 0.06, and 0.6 mg/kg), and in the second animal a PET scan was obtained after the administration of a 2.0-mg dose of ciproxifan per kilogram.

Two animals underwent scans involving the coadministration of doses of GSK189254 aiming to achieve partial occupancy: the first animal underwent 2 scans for which 0.08 μg/kg and 0.25 μg/kg doses of unlabeled GSK189254 were administered. The second animal underwent a similar protocol but with coadministered doses of 0.07 μg/kg and 0.5 μg/kg for GSK189254.

For the challenge experiments, GSK189254 hydrochloride and ciproxifan hydrochloride were dissolved in saline and were intra-

venously injected, immediately followed by the ¹¹C-GSK189254 dose and a saline flush.

Plasma Input Function

Additional arterial blood samples were taken from the femoral artery to determine the total radioactivity concentration in plasma. The samples (a total of 40 per scan) were collected with an automated sampling system for the first 5 min and manually thereafter. In addition, a subset of 18 samples was analyzed for whole-blood activity. The total radioactivity in arterial plasma and blood samples was measured using a γ-counter (Cobra II Auto Gamma; Packard).

Metabolite Analysis

Arterial plasma analysis of ¹¹C-GSK189254 metabolism was performed in all pigs and for each scan. Arterial blood samples (5 mL) were collected at 5, 10, 20, 30, 60, and 90 min after tracer injection. The blood was centrifuged. An equal volume of acetonitrile was added to the plasma sample, and the resulting suspension was then centrifuged at 10,000 rpm for 5 min. The supernatant was removed and filtered through a 0.45-μm nylon syringe filter before HPLC analysis. The deproteinized plasma sample (typically, 1.0–2.0 mL) was injected and analyzed by HPLC with an ultraviolet detector (254 nm) and a flow-through radioactivity detector. Chromatographic separation used a Phenomenex Spherclone ODS column (4.6 × 250 mm), a mobile phase of acetonitrile/ammonium acetate (50 mM; 50/50), and a flow rate of 2.0 mL/min. The fraction of unchanged tracer was determined by the integration of the peak corresponding to the ¹¹C-GSK189254 (retention time, 6.6 min) and expressed as percentage of all the radioactive peaks observed. The input function of arterial blood plasma concentrations corrected for the presence of radiometabolites was generated for all studies. The metabolite correction was performed by fitting a 1-exponential model to the measured parent fraction in plasma.

Kinetic Analysis

Tracer and Challenge Scans. The total volume of distribution, *V*_T, which corresponds to the sum of the specific (*V*_S) and nondisplaceable (*V*_{ND}) components, was derived for each ROI by tracer compartmental analysis. Two models were investigated, the first with a single tissue compartment (1TC) and the second with 2 tissue compartments (2TC). Each model used a fixed delay and blood volume (*V*_B, 5%) (29). The Akaike information criterion (AIC) was used as a metric for parsimonious model selection. In addition, a time-stability analysis was performed by sequentially

examining datasets with decreasing scan durations. This allowed for an assessment of what scanning duration was required to obtain a stable estimate of the volume of distribution in each region.

Homologous Coadministration Scans. The coadministration data were analyzed using a nontracer 2-tissue-compartmental system, which is described by a set of nonlinear differential equations (30). For each scan, the concentration of labeled and unlabeled GSK189254 in the plasma was determined (the unlabeled being derived using the measured specific activity) and used as input functions to the model equations. Time–activity data from the striatum, cortex, and cerebellum in baseline and coadministration scans were fit simultaneously to this model for each animal. The carryover of labeled and unlabeled GSK189254 was accounted for, and parameter estimates (K_1 , plasma clearance; V_{ND} , nondisplaceable distribution volume; $f_{ND}k_{on}$, product of tissue free fraction and the association rate constant; k_{off} , dissociation rate constant; B_{max} , maximum concentration of receptor sites; and V_B , blood volume component) were determined as follows: individual values of K_1 were fitted for each scan and region; B_{max} , V_{ND} , and V_B were held constant across scans but allowed to vary by region; the remaining parameters ($f_{ND}k_{on}$ and k_{off}) were held constant across all scans and regions. Optimization was performed in MATLAB (The MathWorks), and the 18 parameters (9 K_1 , 3 B_{max} , 3 V_B , 1 V_{ND} , 1 $f_{ND}k_{on}$, and 1 k_{off}) were estimated simultaneously for each animal. Estimation of the equilibrium dissociation rate constant $K_d (= k_{off}/k_{on})$ from $f_{ND}k_{on}$ and k_{off} requires an independent estimate of f_{ND} . f_{ND} was estimated under the assumption of passive diffusion using the equation $f_{ND} = f_p/V_{ND}$, where $f_p (=0.46)$ is the GSK189254 plasma free fraction that was determined from an equilibrium dialysis assay.

RESULTS

Radiochemistry

GSK189254 was labeled in the *N*-methyl position by treatment of the carboxamide **1** with ^{11}C -methyl iodide in the presence of tetrabutylammonium fluoride. After a 40-min irradiation time at 40 μA , typical syntheses provided 1.0–2.6 GBq (mean \pm SD, 1.67 ± 0.45 GBq; $n = 14$) of ready-to-inject ^{11}C -GSK189254 at 35 min after the end of bombardment. The incorporation of the ^{11}C -methyl iodide was good, with radiochemical yields of up to 80% based on the trapped ^{11}C -methyl iodide.

Analytic HPLC demonstrated that the radiolabeled GSK189254 was more than 99% radiochemically pure (99.6 ± 0.47 , $n = 14$), with a specific activity of 151 ± 148 GBq/ μmol ($n = 14$). The injected dose of ^{11}C -GSK189254 was 350 ± 136 MBq ($n = 14$), and the

mass dose of unlabeled GSK189254 was 1.28 ± 0.56 μg ($n = 14$).

Lipophilicity

The lipophilicity of GSK189254 was determined to predict its ability to passively cross the blood–brain barrier and the extent of the nonspecific binding signal. The measured $\log D_{7.4}$ of GSK189254 was 1.74 ± 0.03 ($n = 8$).

In Vitro Autoradiography

The incubation of porcine brain sections with 1 nM ^3H -GSK189254 revealed a regional heterogeneous distribution pattern. As illustrated in Figure 2, there was a high level of ^3H -GSK189254 binding in the striatal, cortical, thalamic, hippocampal, and hypothalamic areas and substantia nigra, with minimal binding in the white matter areas, consistent with the results of previous studies conducted using alternative in vitro H_3 radioligands (31,32). Coincubation with the selective H_3 agonist imetit (10 μM) reduced ^3H -GSK189254–specific binding by 90% in the striatal region.

PET in Pig

A sagittal summed (0–90 min) PET image for ^{11}C -GSK189254 under baseline conditions and a structural MR image of a porcine brain are depicted in Figures 3A and 3B. ^{11}C -GSK189254 readily entered the porcine brain; its overall brain uptake was approximately 9.0 %ID/L at 20 min after injection. Typical time–activity curves describing the kinetics of ^{11}C -GSK189254 in the different ROIs and the whole-blood and parent plasma curves are shown in Figure 4A. The regional brain distribution of ^{11}C -GSK189254 reflected the known distribution of the histamine H_3 receptors (1,2,32), with highest accumulation in the striatum, moderate accumulation in the cortices, and low accumulation in the cerebellum.

Metabolite Analysis in Pig

Subsequent to the intravenous administration of ^{11}C -GSK189254, arterial plasma samples were analyzed for labeled parent and metabolites using radio-HPLC. The initial plasma sample displayed a major radioactive peak corresponding to the unmetabolized parent. The fraction of unchanged ^{11}C -GSK189254 in plasma was determined with radiodetection by integration of the peak corresponding to the parent compound as a percentage of the total of all the radioanalytes observed. This percentage decreased from 88% at 5 min after injection to 58% at 30 min after injection

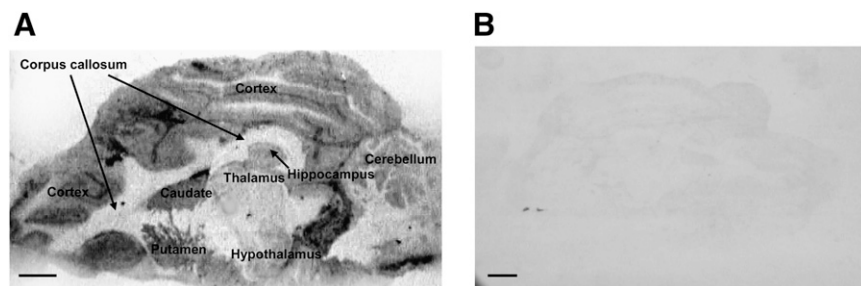


FIGURE 2. (A) In vitro autoradiography of ^3H -GSK189254 (1 nM) binding to H_3 receptors in sagittal sections of porcine brain. Cortex, putamen, caudate, hypothalamus, thalamus, hippocampus, corpus callosum, and cerebellum are indicated. (B) Nonspecific binding was determined in presence of 10 μM imetit.

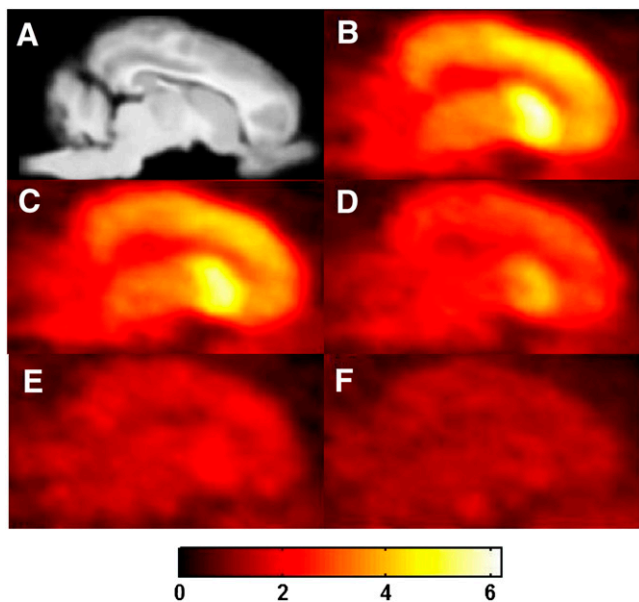


FIGURE 3. Sagittal MR (A) and PET (B–F) images of ^{11}C -GSK189254 binding in porcine brain summed from 0 to 90 min after injection. (A) Aligned MR image. (B) Baseline. (C) +0.006 mg/kg ciproxifan. (D) +0.06 mg/kg ciproxifan. (E) +0.6 mg/kg ciproxifan. (F) +2.0 mg/kg ciproxifan. Scale bar expressed as standardized uptake value.

and then remained stable until the end of the scanning session (55% at 90 min after injection). The major radioactive metabolite observed was more polar than the parent compound and eluted at the solvent front. A second metabolite was observed and was identified as the product of the cleavage of the *N*-cyclobutyl bond. Although the brain permeability of this compound was not investigated, its potential CNS penetration would contribute only to the level of nonspecific binding because this molecule was shown to have no significant affinity at the histamine H_3 receptor (fpKi [recombinant functional assay] < 6.0).

Kinetic Analysis

At baseline, the AIC values for the striatum, cortex, and cerebellum were 141, 143, and 180, respectively, for the 1TC model and 144, 147, and 113, respectively, for the 2TC

model. When a 2 mg/kg dose of ciproxifan was administered, the corresponding AIC values were 166, 148, and 158 for the 1TC model and 97, 93, and 62 for the 2TC model. Regional V_T values obtained using the 2TC model were similar to those obtained using the 1TC model for all regions. For the purpose of brevity, we present only the results from the 2TC analyses. The regional ^{11}C -GSK189254 V_T values in the baseline scan ranged from 5.5 (mL of plasma/cm³ of tissue) for the cerebellum up to 19.8 (mL of plasma/cm³ of tissue) for the striatum (Table 1).

The results of the time-stability assessment of V_T (Supplemental Fig. 1; supplemental materials are available online only at <http://jnm.snmjournals.org>) show that stable estimates of V_T were achieved for all regions by 60 min.

PET with Pharmacologic Challenges

To further characterize the ^{11}C -GSK189254-specific and -nonspecific binding signals, a self-blocking study was performed. Subsequent to a baseline scan, ^{11}C -GSK189254 was coadministered with a dose of unlabeled GSK189254 (50 $\mu\text{g}/\text{kg}$), which blocked the uptake of radiotracer in all H_3 -rich regions, leading to a homogeneous distribution of radioactivity throughout the brain. The corresponding time-activity curves are presented in Figure 4B. To demonstrate the ^{11}C -GSK189254 binding selectivity, a similar blocking experiment was conducted using escalating doses (0.006, 0.06, 0.6, and 2.0 mg/kg intravenously) of ciproxifan. Ciproxifan is a known selective and structurally unrelated histamine H_3 antagonist (14) whose affinity for the histamine H_3 receptor expressed in the porcine cerebral cortex was measured at 9.3 ± 3.6 nM (22). This study showed a dose-dependent decrease of ^{11}C -GSK189254 uptake in the H_3 -rich regions of the brain (Fig. 3). The time-activity curves presented in Figure 5 showed that this dose-dependent decrease of activity uptake was observed in all regions including the cerebellum. The quantification of the ^{11}C -GSK189254 binding confirmed that the administration of ciproxifan induced a significant change in the radioligand V_T in all ROIs (Fig. 6A; Table 1). Moreover, after the coadministration of a 2.0 mg/kg dose of ciproxifan, the V_T values were reduced to similar values throughout the brain, with V_T values ranging from 3.48 to 2.33 mL of plasma/cm³ of tissue for the striatum and cerebellum, respectively,

FIGURE 4. Tissue time-activity curves describing kinetics of ^{11}C -GSK189254 for selected ROIs in porcine brain. (A) Tracer alone. (B) Coadministration of 50 $\mu\text{g}/\text{kg}$ dose of unlabeled GSK189254. \times = striatum; \square = thalamus; \bullet = cortex; \blacktriangle = hippocampus; \circ = cerebellum; * and dotted line = activity corresponding to unmetabolized ^{11}C -GSK189254 in plasma; \diamond and dotted line = total blood activity.

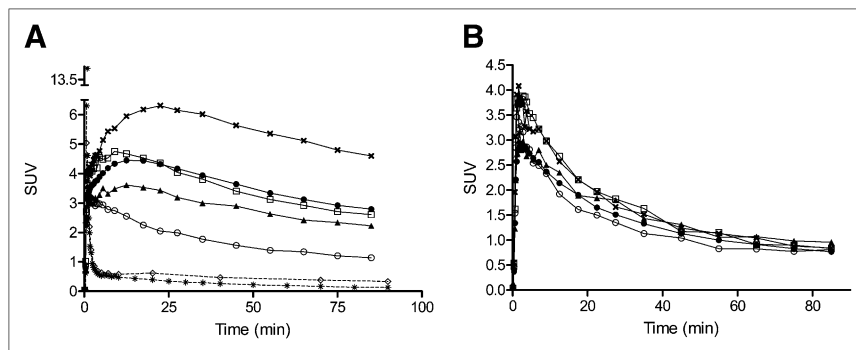


TABLE 1. Receptor Occupancy Estimates from Ciproxifan Competition Study

Dose	Striatum	Cortex	Thalamus	Hippocampus	Cerebellum
Baseline					
V_T	19.8	12.7	10.4	7.9	5.5
BP_{ND}	7.0	4.1	3.2	2.2	1.2
0.006 mg/kg					
V_T	14.1	9.6	8.5	6.7	4.2
BP_{ND}	4.7	2.9	2.4	1.7	0.7
%RO	32.8%	29.5%	24.0%	22.1%	40.9%
0.06 mg/kg					
V_T	9.5	6.9	6.2	5.1	3.7
BP_{ND}	2.9	1.8	1.5	1.1	0.5
%RO	59.3%	56.3%	52.8%	50.6%	58.3%
0.6 mg/kg					
V_T	5.1	4.2	4.3	3.7	2.9
BP_{ND}	1.1	0.7	0.7	0.5	0.2
%RO	85.0%	82.8%	76.7%	77.4%	84.3%
2.0 mg/kg					
V_T	3.5	3.0	3.0	2.4	2.3
BP_{ND}	0.4	0.2	0.2	0.0	-0.1
%RO	94.1%	94.9%	93.7%	100.6%	104.6%

Occupancy and BP_{ND} were estimated using value of V_{ND} (=2.47) derived from blocking study with GSK189254 (50 μ g/kg). All results are derived from 2TC model analyses.
 %RO = $1 - (BP_{ND} \text{ challenge}/BP_{ND} \text{ baseline})$.

demonstrating the specificity of ^{11}C -GSK189254 binding. There was also a significant decrease in the cerebellar V_T values between the baseline scan and the ciproxifan scans, indicating that the cerebellum is not a suitable reference region. Because no region could be regarded as a reference region, the nondisplaceable volume of distribution (V_{ND}) was determined from the cerebellum in the self-blocking study with a 50 μ g/kg dose, when all the H_3 sites were occupied, as $V_{ND} = 2.47$. The ^{11}C -GSK189254 binding potential values were then calculated for each ROI ($BP_{ND} = \frac{V_T - V_{ND}}{V_{ND}}$) (Table 1). The mean occupancy values for the H_3 -rich regions (cortex, striatum, thalamus, and hippocampus) were 27%, 55%, 81%, and 96% when ciproxifan doses of 0.006, 0.06, 0.6, and 2 mg/kg, respectively, were administered.

Similar results were achieved with the ^{125}I TC (data not shown). However, to circumvent the errors that between-subject variability may generate—and, most important, to be able to use ^{11}C -GSK189254 in higher species for which

full blocking experiments may not be achievable and therefore the V_{ND} may not be determinable—a graphical method that obviated a reference region was developed on the basis of work described previously (33–35). This method relied on the availability of several regions with different levels of specific binding and assumed that the occupancy and the V_{ND} were constant for all these regions. Under these circumstances, the following equation can be derived,

$$V_T^{\text{Baseline}} - V_T^{\text{Challenge}} = \text{Occ}(V_T^{\text{Baseline}} - V_{ND}), \quad \text{Eq. 1}$$

where V_T^{Baseline} and $V_T^{\text{Challenge}}$ are vectors of the regional distribution volumes at baseline and after a challenge, V_{ND} is the nondisplaceable distribution volume, and Occ is the occupancy at the target site.

Equation 1 yields a simple graphical representation and linear regression to derive the occupancy (the gradient) and the V_{ND} (the x -intercept). This analytic approach is shown in Figure 6B for the ciproxifan challenge. The receptor

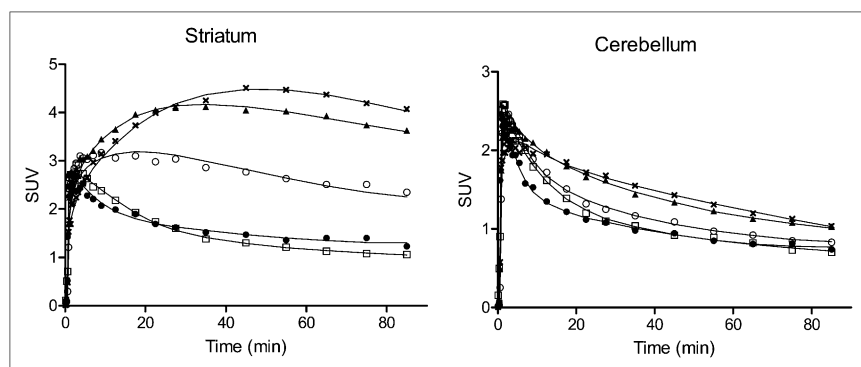


FIGURE 5. Time-activity curves after bolus injection of ^{11}C -GSK189254 in striatum and in cerebellum after administration of escalating doses of ciproxifan. \times = baseline; \blacktriangle = 0.006 mg/kg; \circ = 0.06 mg/kg; \bullet = 0.6 mg/kg; \square = 2.0 mg/kg. Points are measured values, and lines are 2TC model fits.

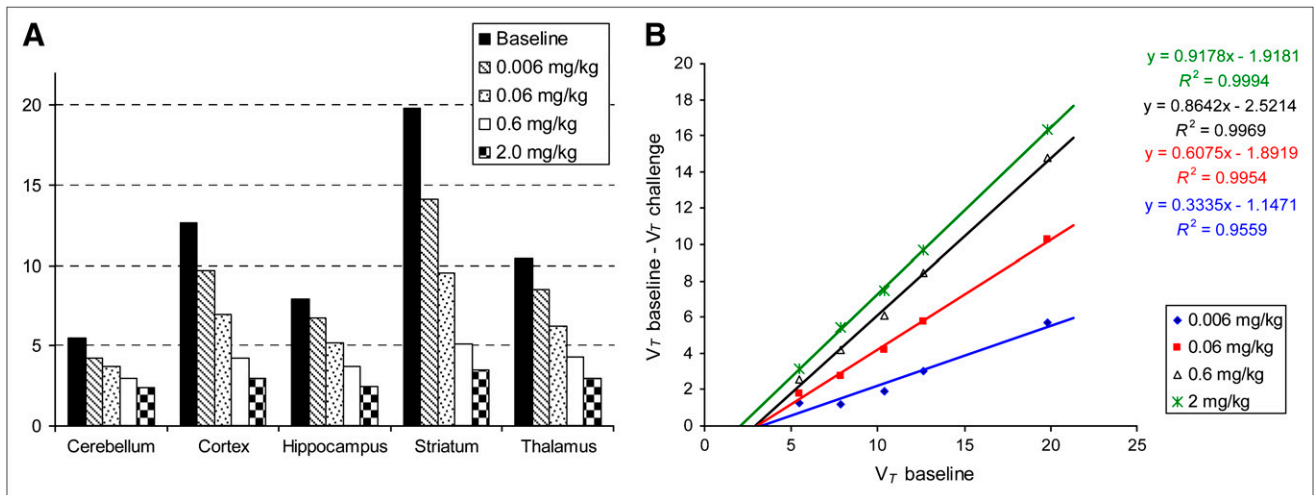


FIGURE 6. (A) V_T estimates from 2TC model before and after treatment with escalating doses of ciproxifan. (B) Graphical interpretation of PET data obtained with 2TC model to estimate receptor occupancy values after administration of escalating doses of ciproxifan.

occupancy values measured using this method were 33%, 61%, 86%, and 92% at 0.006, 0.06, 0.6, and 2 mg/kg, respectively.

Determination of In Vivo Affinity from Homologous Coadministration Experiments

The simultaneous nonlinear fit model (Fig. 7) was able to obtain stable estimates of the parameter values (as determined by independent evaluation from a range of different initial parameter values). The parameter estimates for the tracer affinity and the H_3 receptor concentrations are given in Table 2, and these demonstrate that consistent results were obtained for both subjects. GSK189254 was estimated to have a subnanomolar in vivo affinity (0.09–0.10 nM). The B_{max} estimates for cerebellum (0.5–0.98 nM), cortex (1.4–2.7 nM), and striatum (2.1–3.2 nM) were consistent with the baseline volume of distribution estimates.

DISCUSSION

The aim of this study was to evaluate ^{11}C -GSK189254 as a potential PET radioligand for imaging the histamine H_3

receptor in vivo. 3H -GSK189254 had previously been used for autoradiography studies of the rat brain, demonstrating specific binding in areas such as the cerebral cortex and striatum (22). However, before investigating the binding of ^{11}C -GSK189254 in vivo, autoradiography studies were performed to assess whether the porcine histamine H_3 receptors could be labeled with 3H -GSK189254. 3H -GSK189254 showed specific binding in the porcine brain that correlated with the known distribution of H_3 receptors in the brain. GSK189254 was then labeled with ^{11}C by *N*-methylation in good radiochemical yield and suitable specific activity. Although GSK189254 lipophilicity was slightly below the optimal range of $\log D_{7.4}$ (2.0–3.5) reported for an optimum CNS penetration of drug molecules (36), it was still in the range of known successful PET radioligands (e.g., raclopride and FLB457, $\log D_{7.4} = 1.2$ and 1.6, respectively (26)). A slightly lower $\log D_{7.4}$ may actually be beneficial because it may lead to a lower level of nonspecific binding.

^{11}C -GSK189254 in vivo studies showed high brain penetrance, reversible kinetics, and CNS distribution consistent with the known histamine H_3 receptor location in the

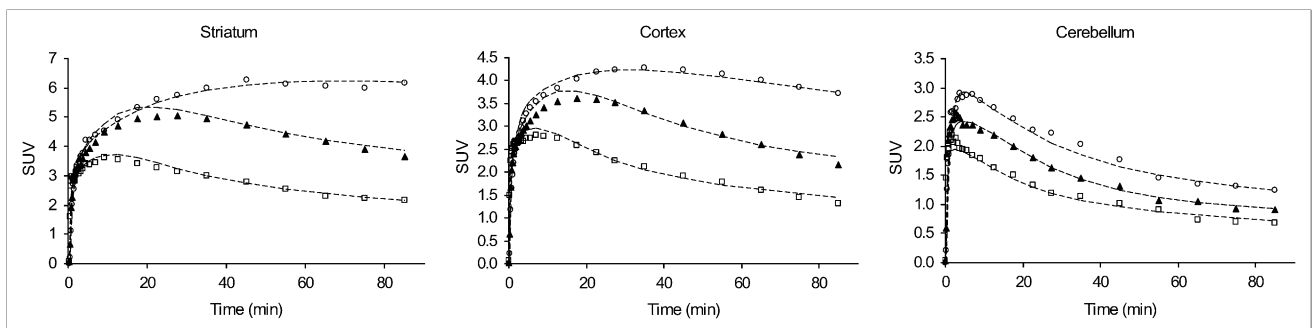


FIGURE 7. Simultaneous nonlinear model fit of time-activity curves of striatum, cortex, and cerebellum for 1 subject for 3 scans. \circ = baseline scan; \blacktriangle = 0.08 $\mu g/kg$ coadministration; \square = 0.25 $\mu g/kg$ coadministration.

TABLE 2. Estimation of In Vivo Affinity of GSK189254 and Regional Concentration Histamine H₃ Sites

Subject no.	Kd (nM)	V _{ND}	B _{max} (nM)		
			Cerebellum	Cortex	Striatum
1	0.09	3.2 ± 1	0.50	1.4	2.1
2	0.10	2.7 ± 0.7	0.98	2.7	3.2

Kd = radioligand affinity.

porcine brain. ¹¹C-GSK189254 was found to have a moderate rate of metabolism in plasma, with around 55% of the parent compound present at 90 min after tracer injection.

According to the AIC, the 2TC model describes the data more appropriately than the 1TC model; however, this difference is less obvious in the baseline scans for regions with high receptor density such as the striatum. This lack of difference at baseline in the striatum can be explained by the free and nonspecifically bound compartment being much smaller than the specifically bound compartment; therefore, for high-binding regions under baseline conditions the kinetic behavior of ¹¹C-GSK189254 can be described with either the 1TC or the 2TC models. When the specific and nonspecific compartments are more comparable after a partial blockade of the receptors, the 2TC model better describes the data.

Time-stability assessment of the V_T showed that a stable measurement was achieved for all regions by 60 min. This was further evidence of the well-behaved reversible kinetics of ¹¹C-GSK189254 in the porcine brain.

In vivo blocking studies with unlabeled GSK189254 and ciproxifan demonstrated that ¹¹C-GSK189254 binding is saturable and is specific to the histamine H₃ receptor binding. The effective binding potentials, BP_{ND}, of 7.0 in the striatum and 4.1 in the cortex confirmed the excellent signal-to-noise ratio of ¹¹C-GSK189254 binding. These blocking experiments also showed that a suitable reference tissue could not be identified and, as a result, a graphical method was developed to determine the percentage of receptor occupancy and to estimate the V_{ND}. The ciproxifan occupancy levels obtained using either the graphical method or the 50 μg/kg GSK189254 block estimate of V_{ND} were consistent, with an average difference of only 5% ± 0.8%.

In the coinjection studies, the estimated in vivo affinity agreed well with the in vitro measurement (0.1 and 0.26 nM, respectively). Moreover, the receptor densities showed the expected rank order according to the known H₃ distribution (striatum > cortex > cerebellum). In addition, the coinjection studies showed that the cerebellum had a small but significant receptor concentration (0.74 nM) and cannot be regarded as a true reference region.

CONCLUSION

These results demonstrate that ¹¹C-GSK189254 is a suitable PET ligand for imaging the histamine H₃ receptor in the pig and warrants translation to humans.

REFERENCES

- Pillot C, Heron A, Cochois V, et al. A detailed mapping of the histamine H₃ receptor and its gene transcripts in rat brain. *Neuroscience*. 2002;114:173–193.
- Anichtchik OV, Peitsaro N, Rinne JO, Kalino H, Panula P. Distribution and modulation of histamine H₃ receptors in basal ganglia and frontal cortex of healthy controls and patients with Parkinson's disease. *Neurobiol Dis*. 2001;8:707–719.
- Arrang JM, Garbarg M, Schartz JC. Auto-inhibition of brain histamine release mediated by a novel class (H₃) of histamine receptor. *Nature*. 1983;302:832–837.
- Clapham J, Kilpatrick GJ. Histamine H₃ receptors modulate the release of [³H]acetylcholine from slices of rat entorhinal cortex: evidence of the possible existence of H₃ receptor subtypes. *Br J Pharmacol*. 1992;107:919–923.
- Schlicker E, Fink K, Hinterthaler M, Goethert M. Inhibition of noradrenaline release in the rat brain cortex via presynaptic H₃ receptors. *Naunyn-Schmiedeberg's Arch Pharmacol*. 1989;340:633–638.
- Schlicker E, Fink K, Detzner M, Goethert M. Histamine inhibits dopamine release in the mouse striatum via presynaptic H₃ receptors. *J Neural Trans Gen Sect*. 1993;93:1–10.
- Leurs R, Blandina P, Tedford C, Timmerman H. Therapeutic potential of histamine H₃ receptor agonists and antagonists. *Trends Pharmacol Sci*. 1998;19:177–183.
- Bray GA, Tartaglia LA. Medicinal strategies in the treatment of obesity. *Nature*. 2000;404:672–677.
- Alguacil LF, Pérez-García C. Histamine H₃ receptor: a potential drug target for the treatment of central nervous system disorders. *Curr Drug Targets CNS Neurol Disord*. 2003;2:303–313.
- Pillot C, Ortiz J, Heron A, Ridray S, Schwartz JC, Arrang JM. Ciproxifan, histamine H₃ receptor antagonist/inverse agonist, potentiates neurochemicals and behavioural effects of haloperidol in the rat. *J Neurosci*. 2002;22:7272–7280.
- Mignot E, Taheri S, Nishino S. Sleeping with the hypothalamus: emerging therapeutics targets for sleep disorders. *Nat Neurosci*. 2002;5:1071–1075.
- Arrang JM, Garbarg M, Lancelo JC, et al. Highly potent and selective ligands for histamine H₃-receptors. *Nature*. 1987;327:111–123.
- Kathmann M, Schlicker E, Marr I, Werthwein S, Stark H, Schunack W. Ciproxifan and chemically related compounds are highly potent and selective histamine H₃-receptor antagonists. *Naunyn-Schmiedeberg's Arch Pharmacol*. 1998;358:623–627.
- Ligneau X, Lin JS, Vanni-Mercier G, et al. Neurochemical and behavioural effects of ciproxifan, a potent histamine H₃-receptor antagonist. *J Pharmacol Exp Ther*. 1998;287:658–666.
- Stark H, Purand K, Huels A, et al. [¹²⁵I]idopropoxyfan and related compounds: a reversible radioligand and novel classes of antagonists with high affinity and selectivity for the histamine H₃ receptor. *J Med Chem*. 1996;39:1220–1226.
- Windhorst AD, Timmerman H, Klok RP, et al. Radiosynthesis and biodistribution of [¹²⁵I]-labeled antagonists of the histamine H₃ receptor as potential SPECT ligands. *Nucl Med Biol*. 1999;26:651–659.
- Windhorst AD, Timmerman H, Klok RP, Menge WMPB, Leurs R, Herscheid JDM. Evaluation of [¹⁸F]VUF 5000 as a potential PET ligand for brain imaging of the histamine H₃ receptor. *Bioorg Med Chem*. 1999;7:1761–1767.
- Ponchant M, Demphel S, Fuseau C, et al. Radiosynthesis and biodistribution of two potential antagonists of cerebral histamine H₃ receptors for PET studies: [¹⁸F]FUB272 and [¹¹C]UCL1829. In: Abstract of papers of the XIIth International Symposium on Radiopharmaceutical Chemistry. June 15–19, 1997; Uppsala, Sweden.
- Airaksinen AJ, Jablonowski JA, van der Mey M, et al. Radiosynthesis and biodistribution of a histamine H₃ receptor antagonist 4-[3-(4-piperidin-1-yl)but-1-ynyl]-[¹¹C]benzyl-morpholine: evaluation of a potential PET ligand. *Nucl Med Biol*. 2006;33:801–810.
- Funaki Y, Sato K, Kato M, Ishikawa Y, Iwata R, Yanai K. Evaluation of the binding characteristics of [¹⁸F]fluoroproxyfan in the rat brain for in vivo visualization of histamine H₃ receptor. *Nucl Med Biol*. 2007;34:981–987.
- Hamill TG, Sato N, Jitsuoka M, et al. Histamine H₃ inverse agonist PET tracers labelled with carbon-11 or fluorine-18 [abstract]. *Neuroimage*. 2008;41(suppl 2):T22.
- Medhurst AD, Atkins AR, Beresford IJ, et al. GSK189254: a novel h₃ receptor antagonist that binds to histamine h₃ receptors in Alzheimer's disease brain and improves cognitive performance in preclinical models. *J Pharmacol Exp Ther*. 2007;321:1032–1045.
- Bjurling P, Reineck R, Westerberg G, et al. *SYNTHIA, a Compact Radiochemistry System for Automated Production of Radiopharmaceuticals: Proceedings of the 6th Workshop on Targetry and Target Chemistry, Vancouver, British Columbia, 17–19 August 1995*. Vancouver, British Columbia; TRIUMF, 1995.
- Bamford MJ, Dean DK, Sehmi SS, Wilson DM, Witherington J, inventors. Glaxo Group Limited, assignee. Benzo[d]azepine derivatives for the treatment of neurological disorders. European patent EP1572215. December 18, 2003.

25. Plisson C., inventor. Glaxo Group Limited, assignee. WO 2006072596 A1. January 6, 2006. 6-(2,3,4,5-tetrahydro-1H-benzo[d]azepin-7-yloxy)nicotinamide derivatives as radiolabelled ligands for the human histamine H3 receptor. International patent application WO 2006/072596 A1. 2006.
26. Wilson AA, Jin L, Garcia A, DaSilva JN, Houle S. An admonition when measuring the lipophilicity of radiotracers using counting techniques. *Appl Radiat Isot.* 2001;54:203–208.
27. Roberts JC, Davis JB, Benham CD. [³H]Resiniferatoxin autoradiography in the CNS of wild-type and TRPV1 null mice defines TRPV1 (VR-1) protein distribution. *Brain Res.* 2004;995:176–183.
28. Watanabe H, Andersen F, Simonsen CZ, et al. MR-based statistical atlas of the Gottingen minipig brain. *Neuroimage.* 2001;14:1089–1096.
29. Gunn RN, Gunn SR, Cunningham VJ. Positron emission tomography compartmental models. *J Cereb Blood Flow Metab.* 2001;21:635–652.
30. Delforge J, Syrota A, Mazoyer BM. Identifiability analysis and parameter identification of an in vivo ligand-receptor model from PET data. *IEEE Trans Biomed Eng.* 1990;37:653–661.
31. Barbier AJ, Berridge C, Dugovic C, et al. Acute wake-promoting actions of JNJ-5207852, a novel, diamine-based H₃ antagonist. *Br J Pharmacol.* 2004;143:649–661.
32. Mezzomo K, Cumming P, Minuzzi L. Comparison of the binding distribution of agonist and antagonist ligands for histamine H₃ receptors in pig brain by quantitative autoradiography. *Eur J Pharmacol.* 2007;564:75–79.
33. Gunn R, Cunningham V, Rabiner E, Slifstein M, Laruelle M. Estimation of occupancy in the absence of baseline data and reference regions [abstract]. *J Nucl Med.* 2007;48(suppl 2):157P.
34. Cunningham V, Gunn R, Rabiner E, Slifstein M, Laruelle M. Graphical analysis of occupancy studies [abstract]. *J Cereb Blood Flow Metab.* 2007;27(suppl 1):53P.
35. Lassen NA, Bartenstein PA, Lammertsma AA, et al. Benzodiazepine receptor quantification in vivo in humans using [¹¹C]flumazenil and PET: application of the steady-state principle. *J Cereb Blood Flow Metab.* 1995;15:152–165.
36. Waterhouse RN. Determination of lipophilicity and its use as a predictor of blood–brain barrier penetration of molecular imaging agents. *Mol Imaging Biol.* 2003;5:376–389.